EFDA–JET–CP(14)06/30

M. Groth, S. Brezinsek, M. Clever, A. Huber, K.D. Lawson, A.G. Meigs,
M.F. Stamp, J. Svensson, S. Wiesen, P. Belo, M. Brix, J.W. Coenen,
C. Corrigan, C. Giroud, C. Guillemaut, D. Harting, S. Jachmich, M. Lehnen,
C.F. Maggi, C. Marchetto, S. Marsen, C. Silva, G.J. van Rooij
and JET EFDA contributors

Steps in Validating Scrape-Off Layer Simulations of Attached and Detached Plasmas in the JET ITER-Like Wall Configuration

Steps in Validating Scrape-Off Layer Simulations of Attached and Detached Plasmas in the JET ITER-Like Wall Configuration

M. Groth[1], S. Brezinsek[2], M. Clever[2], A. Huber[2], K.D. Lawson[3], A.G. Meigs[3], M.F. Stamp[3], J. Svensson[4], S. Wiesen[2], P. Belo[3,5], M. Brix[3], J.W. Coenen[2], C. Corrigan[3], C. Giroud[3], C. Guillemaut[6], D. Harting[2,3], S. Jachmich[7], M. Lehnen[2,8], C.F. Maggi[9], C. Marchetto[10], S. Marsen[4], C. Silva[5], G.J. van Rooij[11] and JET EFDA contributors*

JET-EFDA, Culham Science Centre, OX14 3DB, Abingdon, UK

[1]Aalto University, Association EURATOM-Tekes, Espoo, Finland
[2]IEK4 - Plasma Physics, Forschungszentrum Jülich, Jülich, Germany
[3]CCFE Fusion Association, Culham Science Centre, OX14 3DB, Abingdon, OXON, UK
[4]Max-Planck-Institute for Plasma Physics, EURATOM Association, Greifswald, Germany
[5]Institute of Plasmas and Nuclear Fusion, Association EURATOM-IST, Lisbon, Portugal
[6]Association EURATOM CEA, CEA/DSM/IRFM, Cadarache, France
[7]Association "EURATOM Belgium State", Lab. for Plasma Physics, Brussels, Belgium
8ITER Organisation, 13115 Saint-Paul-Lez-Durance, France
[9]Max-Planck Institute for Plasma Physics, EURATOM-Association, Garching, Germany
[10]Association EURATOM-ENEA, IPP-CNR, Milan, Italy
[11]FOM Institute DIFFER, Association EURATOM-FOM, Nieuwegein, The Netherlands
** See annex of F. Romanelli et al, "Overview of JET Results", (25th IAEA Fusion Energy Conference, St Petersburg, Russia (2014)).*

Preprint of Paper to be submitted for publication in Proceedings of the
25th IAEA Fusion Energy Conference, St Petersburg, Russia
13th October 2014 - 18th October 2014

ABSTRACT

Detailed comparisons of measured and predicted plasma conditions at the divertor target plates and emission across the divertor legs have been carried out with the fluid edge code EDGE2-EIRENE for low-confinement mode plasmas in the JET ITER-like wall materials configuration. In low-recycling scrape-off layer plasma conditions, EDGE2D-EIRENE predicts the measured plasma conditions at the low field side plate, the total radiated power and deuterium Balmer line emission to within 20% WHEN power balance is assumed between the low field side midplane and the low field side divertor plate. In detached conditions the simulations predict 2–3 times lower radiated power and Balmer-α emission, despite achieving electron temperatures of 0.3–0.5eV at the target plates. In the high field side divertor, assumed at least partially detached in low-density upstream conditions the simulations predict Balmer and low charge state beryllium emission closer to the plate than observed experimentally indicating hotter plasma conditions in the simulations. Our studies show that radiation from beryllium and carbon cannot explain the observed radiation deficit.

1. INTRODUCTION

Operation in partially detached divertor conditions is mandatory in ITER and in other future, tokamak-based fusion reactors. The primary purpose of detached divertor operation is to preserve the integrity of the divertor plasma-facing components while simultaneously to maintain sufficiently high plasma purity for fusion power production. Fully detached and strongly recombining divertor plasmas close to the density limit were systematically characterised experimentally in JET in the ITER-like wall (JET-ILW) materials configuration and in a diagnostic-optimised divertor plasma configuration (Figure 1 of ref. [1]). These studies are complemented by identical measurements in attached and partially detached divertor plasmas. Low confinement mode (L-mode) plasma conditions were chosen to reduce the level of complexity and plasma dynamics associated with edge localised modes (ELMs) in high confinement (H-mode) plasmas. The reduction of carbon as the primary plasma impurity and thus radiator, previously reported in [2], and carbon chemistry in plasma-wall interaction, greatly simplified the assessment of the role of deuterium in removing momentum and power from the plasma to achieve detachment. Low concentration of low charge state impurities, such as beryllium and carbon, still observed in the plasma is used for diagnosis of the plasma conditions. Previous simulations with the edge fluid code EDGE2D, coupled to the neutral Monte Carlo code EIRENE ([2], EIRENE version 2008 [4]) showed that elastic collisions of deuterons with deuterium molecules play a key role in reducing the plasma temperature in front of the target plate to below 1eV, resulting in an up to fourfold reduction of the ion currents to the low field side (LFS) plate [1],[5]. However, the total radiated power spatially integrated over the scrape-off layer (SOL) was predicted to be two times lower than inferred from tomographic reconstructions of the bolometry data.

To further characterise the radiation shortfall, comparisons of EDGDE2-EIRENE predictions with line-integrated bolometer and spectroscopic signals and imaging spectroscopy using tangentially

viewing cameras are carried out. Building upon previous EDGE2D-EIRENE simulations [1], these runs were extended to include cross-field drifts (**E**x**B**, **B**x∇B, diagmagnetic and curvature drifts) for pure-deuterium (pure-D), and carbon as a second impurity to beryllium (D+Be+C) in runs without cross-field drifts. Beryllium is considered a non-recycling species sputtered by deuterium and beryllium (self-sputtering) atoms and ions using yields calculated by SDTrimSP [6]. In the D+Be+C simulations, carbon is treated as an extrinsic and recycling species. It was injected from the wall adjacent to the private flux region and removed by 'EIRENE pumps' in the divertor corners. The injection rate is feedback-controlled on the user-set total carbon radiation within the computational domain. Tungsten was omitted in the simulations due to alleviate excessive computational time; it was previously shown that tungsten is not a significant radiator in the SOL for these plasmas (Figure 10 of [1]). The input parameters, transport models, EIRENE model, and boundary conditions are kept identical to those in [1]. To characterise the difference of attached versus detached divertor conditions, one low-recycling and one partially-detached case at the LFS divertor plate are investigated. The electron density at the LFS midplane separatrix, $n_{e,sep,LFS\text{-}mp}$, was determined for the lowest core plasma density case by assuming power balance between the LFS midplane and the LFS target plate [Pitcher_PPCF97], resulting in systematic shifts of the separatrix relative to the measured density and temperature profiles of up to 1.5 cm for these JET plasmas [8]. Because of the uncertainty of this methods, in particular at high core plasma densities, systematic scans of $n_{e,sep,LFS\text{-}mp}$ and of the power crossing the EDGE2D-EIRENE core boundary were performed to assess the sensitivity of the predicted synthetic diagnostics and their comparisons to the measurements [1].

2. ASSESSMENT OF LINE EMISSION CONTRIBUTIONS TO TOTAL RADIATED POWER

The largest contribution of (line) emission to total radiated power is estimated to be due to deuterium Lyman (Ly) emission, in particular from Ly-α [9]. In divertor plasmas of densities from 10^{19} to $10^{20}m^{-3}$ and corresponding temperatures from 10eV to 2eV, Ly-α approximately accounts for 85–90% of the total deuterium radiation, about 10% in Ly-β, and about 3% in the other atomic deuterium lines (see table 1 in [9]). Line radiation from deuterium molecules is estimated to be of the order 3–10% of the atomic deuterium lines, and radiative recombination of deuterons followed by cascading and Bremsstrahlung of up to 30% at the highest densities and lowest temperatures. Given the low effective plasma charge (Z_{eff}, $Z_{eff} \approx 1.1$ at densities close to density limit), impurities are predicted to contribute as little as a 1% for beryllium and 0.1% for carbon [2].

3. IMPACT OF CROSS-FIELD DRIFTS ON PLASMA CONDITIONS, TOTAL POWER AND DEUTERIUM EMISSION

Inclusion of cross-field drifts in pure-D EDGE2D-EIRENE cases increases the total radiated power in the computational domain, $P_{rad,tot,E2D}$, by 30% for the low $n_{e,sep,LFS\text{-}mp}$ case, and by 15% for the high $n_{e,sep,LFS\text{-}mp}$ case (table 1). Poloidally, the increase in $P_{rad,tot,E2D}$ is most significant in the HFS

divertor region (Figure 1a and b), which also shows an increase in deuterium Balmer-α (D-α) at the HFS plate (Figures 1c and d), and a reduction of the electron temperature (T_e) at the HFS strike zone (Figures 1e and f). The change in plasma conditions, line emission and thus total radiated power is consistent with the direction of the poloidal $\mathbf{E_r}$x$\mathbf{B}$ drifts in the private flux region from the LFS to the HFS divertor, as observed experimentally [10] as well as in edge fluid simulations [11], [12], [13]. Since the divertor plasma temperatures are higher in the low $n_{e,sep,LFS\text{-}mp}$ case, and thus the radial electric field, E_r, the effect is more pronounced in low-density cases.

For the low $n_{e,sep,LFS\text{-}mp}$ case, the plasma conditions along the LFS plates, and the D-α and D-γ emissions across the LFS divertor are consistent with the measured profiles to within 20% (Figure 1a,c,g). The predicted peak T_e at the HFS plate decreased from 60eV to 30eV (Figure 1e) and the peak D-α emission across the HFS divertor leg nearly tripled (Figure 1c). The plasma conditions at the LFS plate and the radiation across the LFS leg are insensitive to the inclusion of drifts (Figure 1c, g). The divertor plasma is predicted to be in low recycling conditions as inferred from the measurements. Assuming a line-integrated radiated power of 10kW/m^2 from the core, which is not accounted for in the EDGE2D-EIRENE computational domain, also the predicted profile of the total radiated power across the LFS divertor as agrees with the measurements (Figure 1a). The discrepancy in total radiated power arises from the HFS divertor leg, which is measured to be more strongly radiating by factors of 3 to 5 than what is predicted. Furthermore, the calculations put the D-α emission peak at the HFS divertor plate, while it is well off the HFS plate in the simulations.

For the high $n_{e,sep,LFS\text{-}mp}$ case, the plasma conditions along the LFS plates are predicted to be cold ($T_e \approx 0.5$–0.8 eV) and detached across the entire plate (Figure 1h). However, the radiation produced in these plasmas is lower by 2 to 3 compared to the measured total radiation (Figure 1b), D-α (Figure 1d) and D-γ emissions (not shown). Since there is still a radiation deficit, the divertor plasma may be assumed even colder than predicted. Analysis of the Langmuir probe data following Gunn et al. [14] still produces $T_e > 5$eV, which is inconsistent with high-n Balmer line analysis and imaging of low charge state carbon emission. The discrepancy between predicted total radiation and D-α emission across the HFS divertor is exacerbated compared to the LFS divertor, pointing at the same inaccurate physics model or database that produces the radiation shortfall. It is interesting to note that EDGE2D-EIRENE shows cold, partially detached regions at the separatrix and along the vertical face of the HFS plate, and an increase in T_e in the common flux region at $R\text{-}R_{sep,LFS\text{-}mp}$, where the divertor geometry changes from vertical to approximately 45-degree inclination.

4. ASSESSMENT OF LINE EMISSION FROM LOW-Z IMPURITIES AND THEIR CONTRIBUTION TO $P_{RAD,TOT}$

To address the impact of beryllium as the primary intrinsic plasma impurity species, and carbon as a secondary species on total radiation, the poloidal distributions of line emission and the plasma conditions at the plates, EDGE2D-EIRENE was executed without cross-field drifts, but otherwise identical models. (The code was successfully run with drifts and beryllium for intermediate values

of $n_{e,sep,LFS\text{-}mp}$, however, was numerically unstable for both the low and high end of $n_{e,sep,LFS\text{-}mp}$).

Introducing Be as plasma species sputtered at the main chamber wall only raises $P_{rad,tot,E2D}$ by about 50% for the low $n_{e,sep,LFS\text{-}mp}$ case, and by 15% for the high $n_{e,sep,LFS\text{-}mp}$ case over the pure-D case (table 1). Introducing C as a recycling impurity and aiming at 'calibrating' the total radiated power in carbon against the measured CII emission at 427nm across the LFS divertor, $P_{rad,tot,E2D}$ was raised further by about a factor of 2 for the low $n_{e,sep,LFS\text{-}mp}$ case, and by 25% for the high $n_{e,sep,LFS\text{-}mp}$ case compared to the pure-D case. To reproduce the measured CII emission, a total of 100kW of carbon radiation was required for the low $n_{e,sep,LFS\text{-}mp}$ case (Figure 2g); this feedback power request was then also applied to the high $n_{e,sep,LFS\text{-}mp}$ resulting in 2-3 times higher CII emission than measured (Figure 2h). To reproduce CII emission for the high $n_{e,sep,LFS\text{-}mp}$ case, 50kW of carbon radiation may have sufficed. Hence, radiation in Be and C is insufficient to raise $P_{rad,tot,E2D}$ to the magnitude observed in the experiments, in particular in detached divertor plasmas.

Introducing Be and C predominately raised the total radiation across both the HFS and LFS divertor legs for the low $n_{e,sep,LFS\text{-}mp}$ case (Figure 2a) and across the LFS divertor leg for the high $n_{e,sep,LFS\text{-}mp}$ case (Figure 2b). It has little to no effect on the plasma conditions at the HFS and LFS plates (not shown) and the D-α emission across the divertor legs (Figure 2c,d). Allowing Be to be sputtered in the main chamber only, and no recycling at the main chamber wall and divertor targets, the simulations do not predict significant BeII emission due to Be ions being transported into the divertor (Figure 2e and f).

Assuming a pure Be divertor with sputtering yields of 5% of those calculated by SDTrimSP [6] at the HFS and LFS plates, $P_{rad,tot,E2D}$ increased by about a factor of 1.5 over the pure-D case at low $n_{e,sep,LFS\text{-}mp}$, and by 30% at high $n_{e,sep,LFS\text{-}mp}$. The primary motivation of this assumption was to raise $P_{rad,tot,E2D}$ to the level measured with the poloidally scanning divertor spectrometer across the HFS divertor (Figure 2e). Due to change in contributions from recycling deuterium atoms versus molecules – higher number of molecules in the case of a low-Z (Be) versus a high-Z (W) surface [15] – T_e at the HFS and LFS plate is further reduced. For the low $n_{e,sep,LFS\text{-}mp}$ case, T_e at the LFS strike point was reduced from 60eV to 40eV. This process effectively leads to an increase in total radiated power (Figure 2a) and D-α emission (Figure 2c) across the LFS divertor leg. The BeII emission, however, then exceeds the measured emission by a factor of 4, For the high $n_{e,sep,LFS\text{-}mp}$ case, significant BeII emission is predicted from the far SOL at the LFS divertor, likely due to Be sputtering by charge exchange neutrals along the vertical face of the LFS divertor. Both predictions for BeII emission are inconsistent with the BeII measurements and post-mortem analysis [16], and indicate that the divertor plasma face a tungsten divertor, at least at the LFS side.

5. ASSESSMENT OF DEGREE OF RECOMBINATION IN DETACHED PLASMAS

Despite the shortfall of total radiation and D-α emission, comparisons of measured and predicted line emission from high-n Balmer transitions (D10-2) show for the high-density case ($n_{e,sep,LFS\text{-}mp} = 1.8 \times 10^{19} m^{-3}$) that recombination is a significant process in the LFS divertor plasmas [17], and that

this process is accounted for in the simulations (Figure 3). The population of such high electronic levels show that along the sightline of the spectrometer a significant region of the plasma is below 1eV, and that this region is radially inboard of the LFS strike zone. The same observation was made and conclusion drawn from measurements and EDGE2D-EIRENE simulations in high-triangularity L-mode plasmas [5]. Simulations including cross-field drifts predict the profile to be shifted radially inward and further extended, bringing the predictions into closer agreement with the measurements.

6. 2D DISTRIBUTIONS OF D-A AND CIII LINE EMISSION IN THE DIVERTOR

The predicted 2-D poloidal profiles of D-α line emission in the divertor show for the high density case ($n_{e,sep,LFS\text{-}mp} = 1.8 \times 10^{19} m^{-3}$) the emission being extended into the divertor plasma both on the HFS and LFS, while the measurements reveal more localised emission at the strike points [18] (Figure 4.). Simulations in pure-D with the drifts included (Figure 4c) indicate emission farther into the divertor X-point region than their corresponding no-drift cases (Figure 4b). Emission from low charge state carbon ions (CIII at 465nm) was inferred to be highly localised at the divertor X-point, indicating that cold ($T_e < 8eV$) divertor legs from the X-point to the divertor plates. EDGE2D-EIRENE simulations including carbon, but not cross-field drift, also predict the peak emission off the divertor target plates (Figure 4e), further substantiating that much of divertor plasma is below 10eV. The measured profiles (Figure 4a, c) were calculated from images of a wide-angle, tangentially-viewing camera system [19] and reconstructed from 3-D into 2-D poloidal plane by non-parametric tomography using Gaussian processes [20].

7. SUMMARY

Detailed analyses of EDGE2D-EIRENE simulations for total radiated power, and deuterium, beryllium and carbon emission in JET ILW L-mode plasmas indicate a significant deficit in radiation in the SOL compared to the measurements. This radiation deficit is more pronounced in detached plasmas and is observed in both divertor legs, when detached. For low recycling plasmas, forcing upstream-downstream power balance along **B**, and adjusting the radial diffusivities to replicate the measured profiles, reproduces the measured target profiles of ion flux and electron temperature, and the D-α and D-γ emission profiles across the divertor legs to within 20% of their measurements. Inclusion of cross-field drifts in pure-D simulations raises the total radiation and D-α emission in the HFS divertor leg. However, the predicted peak of D-α remains at the HFS plate, and is not located between the HFS plate and HFS X-point region as observed experimentally. On the other hand, when the divertor plasma is fully detached (at the LFS plate) the simulations do predict emission from high-n Balmer lines to the extent observed experimentally, which would imply that the magnitude of recombination in the LFS divertor leg is correctly captured. The simulations also indicate that divertor geometry and plate alignment play a role in detaching first at the separatrix and then in the mid and far SOL.

Replicating the measured CII emission across the LFS divertor leg, the simulations show that the remaining carbon in JET-ILW is not a significant radiator affecting the SOL power balance. Similarly, imposing a beryllium divertor overestimates the measured emission from low charge state beryllium, even when reducing the beryllium yields to 5% of those published. The divertor plasma is predicted to cool when switching from W to Be surfaces, due to preferential released of deuterium as molecules off low-Z surfaces.

The predictions of the divertor conditions and subsequent radiated power strongly depend on the assumed separatrix density and power crossing the domain core boundary. Since the separatrix location is uncertain to within 1cm, or up to $3 \times 10^{18} m^{-3}$, $n_{e,sep,LFS\text{-}mp}$ remains a too unconstrained free parameter in the simulations. In detached conditions deuterium molecules and molecular ions are expected to play a significant role in removing power, in addition to momentum. Present experimental investigations focus on detailed measurements of molecules and their contributions to total recycling flux, and on verification and validation of these processes in EDGE2D-EIRENE.

ACKNOWLEDGMENT

This work was supported by EURATOM and carried out within the framework of the European Fusion Development Agreement (EFDA). This work has also been carried out within the framework of the EUROfusion Consortium and has received funding from the European Union's Horizon 2020 research and innovation programme under grant agreement number 633053. The views and opinions expressed herein do not necessarily reflect those of the European Commission.

REFERENCES

[1]. Groth, M. et al., Nuclear Fusion **53** (2013) 093016.
[2]. Brezinsek, S. et al., Journal of Nuclear Materials **438** (2013) S303.
[3]. Wiesen, S., ITC-Report, http://www.eirene.de/e2deir_report_30jun06.pdf (2006).
[4]. Kotov, V. et al., Plasma Physics and Controlled Fusion **50** (2008) 105012.
[5]. Guillemaut, C. et al., Nuclear Fusion **54** (2014) 093012.
[6]. Mutzke, A. et al., IPP report 12/8, April 2011: http://edoc.mpg.de/552734
[7]. Pitcher, C.S. et al., Plasma Physics and Controlled Fusion **39** (1997) 779.
[8]. Groth, M. et al., Journal of Nuclear Materials **438** (2013) S175.
[9]. Lawson, K.D. et al., submitted Journal of Nuclear Materials 2014.
[10]. Boedo, J.A. et al., Physics of Plasmas **7** (2000) 1075.
[11]. Aho-Mantila, L. et al., this conference.
[12]. Chankin, A.V. et al., Journal of Nuclear Materials **241–243** (1997) 199.
[13]. Porter, G.D. et al., Physics of Plasmas **7** (2000) 3663.
[14]. Gunn, J. et al., Review of Scientific Instruments **66** (1995) 154.
[15]. Järvinen, A. et al., this conference.
[16]. Heinola, K. et al., submitted Journal of Nuclear Materials 2014.

[17]. Meigs, A.G. et al., Journal of Nuclear Materials **438** (2013) S607.
[18]. Clever, M. et al., Proceedings 41st EPS conference, Berlin, Germany, 2014.
[19]. Clever, M. et al., Fusion Engineering and Design **88** (2013) 1342.
[20]. Svensson, J. submitted to Inverse Problems 2014.

Cases \ $n_{e\,sep\,LFS\text{-}mp}$	0.8×10^{19} m^{-3}	1.8×10^{19} m^{-3}
Experiment	5.3×10^{5} W ± 5×10^{4} W	1.1×10^{6} W ± 1×10^{5} W
Pure-D	9.25×10^{4} W	5.10×10^{5} W
Pure-D + drifts	1.28×10^{5} W	5.72×10^{5} W
D+Be	1.40×10^{5} W	5.88×10^{5} W
D+Be+Be div (5%)	2.37×10^{5} W	6.69×10^{5} W
D+Be+C (100 kW)	1.98×10^{5} W	6.47×10^{5} W

Table 1: Total radiated power across the EDGE2D-EIRENE computational domain and its equivalent for the measurements for 5 sets of assumptions in the simulations.

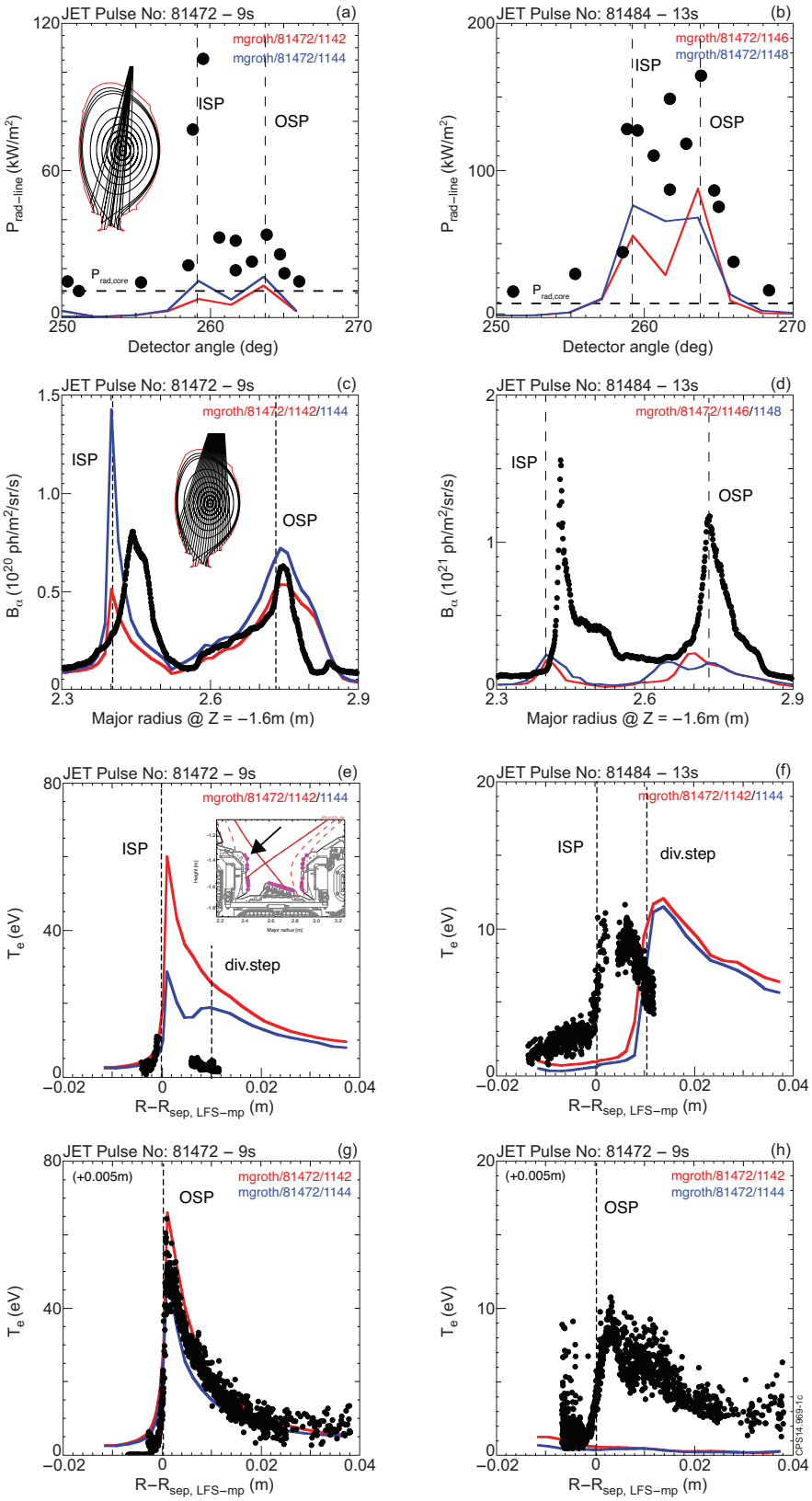

Figure 1: Measured (black symbols) and predicted radiated power along the JET bolometer lines-of-sight (vertical system only, a, b), D-α emission along the lines-of-sight of a poloidally scanning divertor spectrometer (c, d), and Langmuir probe T_e profiles along the HFS (e, f) and LFS (g, h) target plates. The data is shown for a low recycling plasma (ne, sep, LFS–mp = 0.8 × 10 m^{-3}, left column), and a partially detached plasma (ne, sep, LFS–mp = 1.8 × 10 m^{-3}, right column) The EDGE2D-EIRENE predictions are for pure-D plasmas without drifts in red and with drifts in blue. The D-α emission is calculated from electronic transitions only, i.e., vibrational-rotational states are omitted.

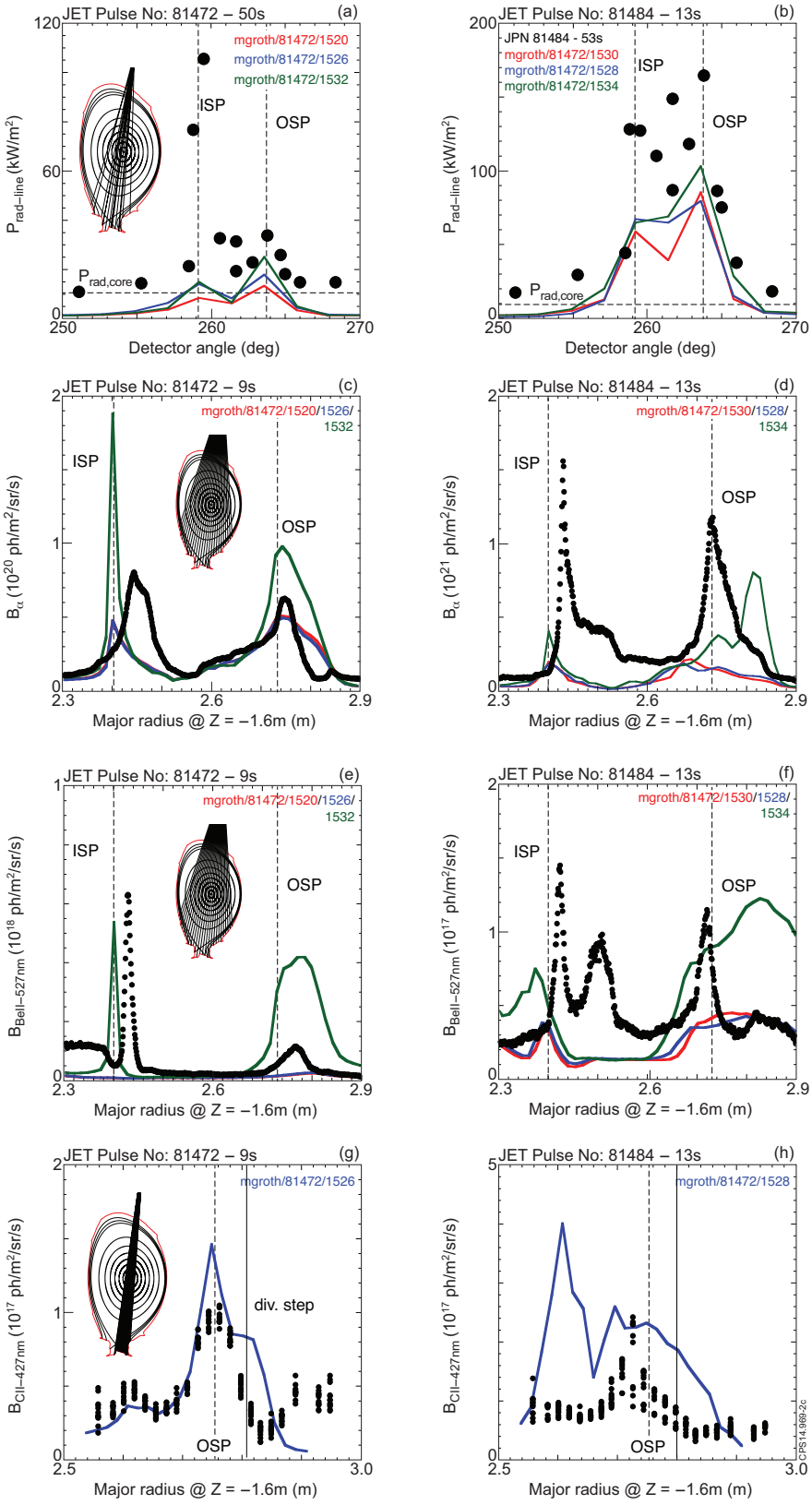

Figure 2: Measured (black symbols) and predicted radiated power along the JET bolometer lines-of-sight (vertical system only, a, b), D-α (c, d) and BeII at 527nm (e, f) along the lines-of-sight of a poloidally scanning divertor spectrometer, and CII line emission at 427nm along the lines-of-sight of a high-resolution divertor spectrometer (g, h). The data is shown for a low-recycling plasma (ne, sep, LFS-mp = 0.8 × 10 m^{-3}, left column), and a partially detached plasma (ne, sep, LFS-mp = 1.8 × 10m^{-3}, right column) The EDGE2D-EIRENE predictions are no-drift cases for D + Be (red), D + Be + C (blue) and a Be divertor assuming 5% of the published physical sputtering yields (green).

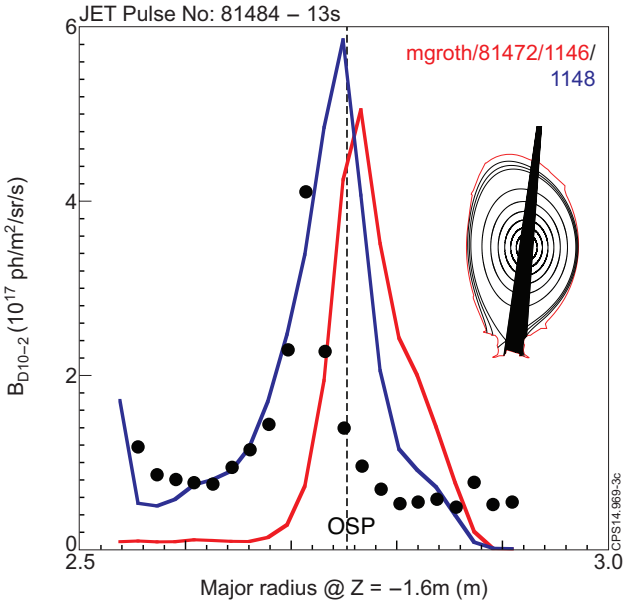

Figure 3: Poloidal profiles of the line-integrated Balmer emission of the n = 10 → 2 transition. EDGE2D-EIRENE predictions are shown for pure-D cases with (red) and with (blue) cross-field drifts.

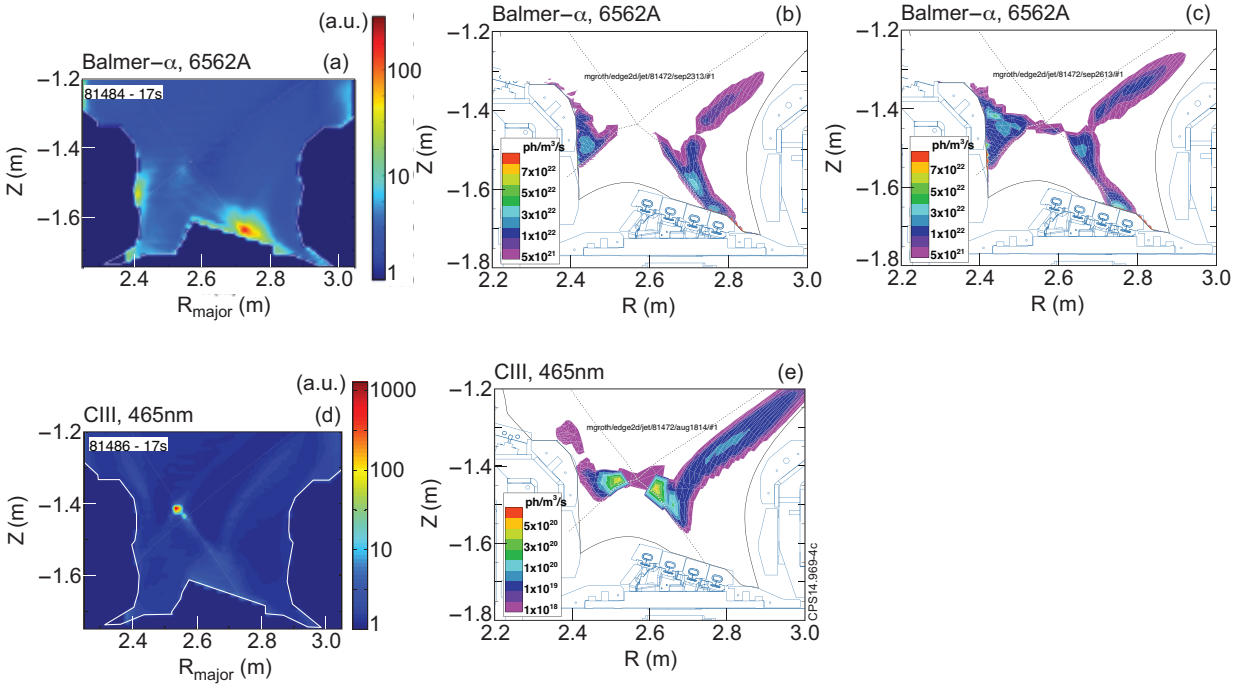

Figure 4: Measured (a, d) and predicted 2-D emission profiles of emission at D-α (a-c) and CIII 465nm (d, e).